Journal of Marine Science and Technology
https://doi.org/10.1007/s00773-018-0600-0

Optimization-Based Motion Planning for Trawling

Joakim Haugen · Lars Imsland

Received: 4 April 2018 / Accepted: 20 September 2018

Abstract This work presents an optimization-based motion planning system for trawling operations. The formulation makes use of simplistic physical descriptions of the vessel and fishing gear together with catch dynamics of sweeping across moving fish schools. The objective of the optimal control problem is to maximize harvest, while ensuring both feasible maneuvers and well-behaved gear characteristics. The problem is transcribed into a large-scale nonlinear programming problem and solved in a receding horizon fashion using simultaneous collocation. A numerical simulation illustrates the system's usefulness.

Keywords Marine robotics · Trawling · Predictive control.

1 Introduction

Pelagic trawling is a complicated operation that involves continuous intervention from operators. Decisions, such as how to maneuver the vessel for efficient harvest and which region to explore next, require insight to make. Modern fishing vessels are equipped with various instruments and equipment that provide operators with useful information about the vessel and the environment. The volume and velocity at which the information are made available may take its toll on the operators. Consequently, it is demanding for operators to sufficiently process this information and make decisions that align with the short-term objectives of the operation. Also, the impact of short-term decisions in the long run is often not immediately clear. This work proposes a system that tries to alleviate some of the workload on the operators by using model predictive techniques in a vessel and fishing gear motion planning problem. In particular, we want to autonomously produce feasible trajectories for both the vessel and trawl net, given information about fish schools' motion and characteristics.

There exists some work on path-tracking controllers for trawling, including approaches based on model predictive control [1], and fuzzy controllers [2–5]. Controllers may help in performing trawl maneuvers prescribed by the skipper [6], but there is a human-in-the-loop component in such a paradigm. Literature on autonomous motion planning for trawling operations, on the other hand, is sparse.

Motion planning (see e.g. [7]) in general has a huge body of literature, finding applications in various fields, including driverless cars, robot navigation, path planning for target tracking, or dynamic coverage control. The work herein finds similarities to path planning for *target tracking* [8], and in particular approaches using dynamic vehicle models combined with information-driven reward functions of visiting objects or regions [9,10]. The notable difference from previous works is the inclusion of an actuator removed from the rigid body configuration of the moving vehicle. The location of the actuator is connected to the vehicle through a link, but there is no direct control of the link's angular configuration in relation to the vehicle's motion. The motion planning of the net thus needs to rely on manipulation of both the vessel's motion and the link's length. The

J. Haugen
SINTEF Ocean, Trondheim, 7465 Norway
Tel.: +47-930-33-792
E-mail: joakim.haugen@sintef.no

L. Imsland
Department of Engineering Cybernetics, NTNU, Trondheim, 7491 Norway
Tel.: +47-735-94-349
E-mail: lars.imsland@ntnu.no

main contribution of this work is the formulation of an optimal control problem that finds feasible trajectories for both the vessel and the net in order to catch fish autonomously.

Mathematical models involved in describing a trawl operation are discussed in [1, Section 1.2.3]. Most components can be modeled with high-fidelity, but at high computational requirements. General cable models with internal and external forces, such as gravity and hydrodynamics can be used to describe bridles, warps, and other cable-like parts of the gear, see e.g. [11]. Trawl doors function as hydrofoils and are often described using experimental data to parameterize the drag, lift, and shear coefficients of the model [1]. Several methods for constructing models for trawl nets exists, including finite element approaches with super meshes [12], mass-lumped models [13], and interconnected rigid bar models, see [1] and references therein. Hydrodynamic loads are complex to evaluate due to hydroelasticity [14]. Models for vessel maneuvering is covered in [15].

2 Problem Overview

A pelagic trawling operation consists of a fishing vessel that drags a submerged trawl net in mid-water, well clear of the seabed. In a single trawl, the net is connected to two trawl doors via so-called bridles (wires). The doors' task is to ensure that the net stays open, backed by a floating head line and sinking fish line. The doors are connected to winches on board the vessel via warps (wires). The objective of the trawling operation is to catch fish by sweeping the net opening through fish schools by manipulating the vessel's motion and the warp lengths. See Fig. 1 for a pictorial overview of the main components in mid-water trawling.

During trawling, the operators are aided by a fish finding sonar. The sonar provides periodic snapshot images of what may be fish schools. This information is then used by the operator to determine vessel trajectories and warp lengths in order to achieve sweeps through schools, while at the same time obeying maneuverability constraints and preserving well-behaved gear characteristics. Herein, our task is to propose a motion planning system that mimics this operation and thereby facilitates an autonomous trawling system.

Dynamic Catch Planning The vessel and fishing gear serve as a mobile actuator on the environment, which includes fish schools. Sensor measurements of the gear and the environment are feedback for deciding subsequent actions. The motion planning component, denoted *Dynamic Catch Planner*, is responsible for autonomously determining appropriate vessel and net trajectories. The objective of the planner is to catch fish in an efficient and safe manner. The operators supervise the motion planning and may provide overriding commands or, if necessary, take over the operation. Fig. 2 depicts a diagram of the main components in the proposed system. We proceed by defining a *Path Planner*, which is part of the *Dynamic Catch Planner*, and demonstrate its usefulness in a numerical simulation, which is provided in Section 4.

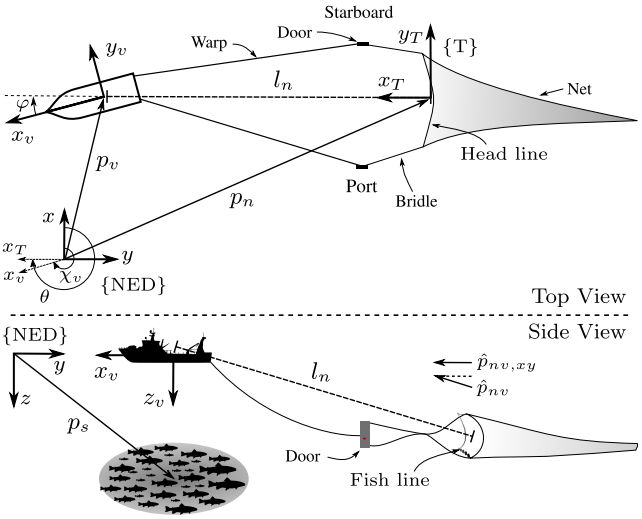

Fig. 1 Trawling involves of a fishing vessel, warps, doors, bridles, head line, fish line, trawl net, and fish schools. The coordinate systems and variables are explained in throughout the manuscript.

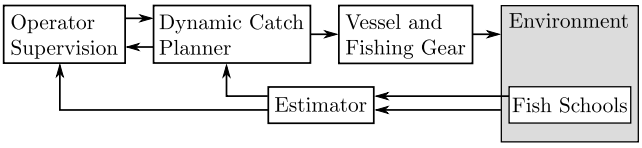

Fig. 2 A diagram with the main components in the proposed system.

3 Path Planner

When a sector is being harvested, the tactical planning entails producing trajectories that are feasible with respect to the maneuverability constraints of the fishing vessel. This task includes constructing paths that are sufficiently conservative, which in turn makes sure that the fishing gear behaves appropriately during maneuvering. The purpose of the maneuvering is to maximize harvest of fish.

There are several principal components that dictate the behavior of the harvest operation. If one can describe these components with sufficient fidelity, perhaps the insight can be used in automating the tactical har-

vest. We identify the following key components of the harvest operation:

A. Fishing vessel;
B. Fishing gear;
C. Fish schools;
D. Trawl catch dynamics;
E. Fish harvest indication.

The rationale behind the component models is to provide a simple and computationally efficient *control plant* model for a *Path Planner*. The *Path Planner* combines descriptions of the above components to predict future behavior – the purpose is to device a sound course of action. We will later see that the planning algorithm employs a periodic re-planning scheme, so the combined model does not need to accurately describe the operation for long time periods, as long as it retains the system's main response. We proceed by mathematically modeling the components just listed, before arriving at the combined system and the *Path Planner*'s dynamic optimization problem formulation. An overview of variables with descriptions, which will be defined throughout the manuscript, has been added in Appendix A.

3.1 Fishing Vessel

We model the fishing vessel as a planar kinematic vehicle. Let {NED} denote an inertial reference frame with the axes x, y, and z pointing north, east, and down, respectively. Define $p_v(t) \in \mathbb{R}^2$ as the planar position of the vessel, situated on the xy-plane of {NED}. Further, let $\chi_v(t) \in \mathbb{R}$ be the course of the vessel, that is, the angle of the vessel's velocity vector relative to the x-axis, following the right-hand screw rule. $U > 0$ is the constant speed of the vehicle model. We get the following vehicle model with limited turn rate

$$\dot{p}_v(t) = U \begin{bmatrix} \cos \chi_v(t) \\ \sin \chi_v(t) \end{bmatrix}, \tag{1a}$$

$$\dot{\chi}_v(t) = u_v(t), \tag{1b}$$

$$p_v(t_0) = p_{v,0},\ \chi_v(t_0) = \chi_{v,0}, \tag{1c}$$

where $u_v(t) \in [u_{v,\min}, u_{v,\max}] =: \mathbb{U}_v$ is a constrained control input. The constant speed property can easily be relaxed, either letting acceleration or speed itself be a control input. For future reference, define the 3-dimensional expressions for the vehicle's position and velocity as $\bar{p}_v(t) = \text{col}(p_v(t), 0)$ and $\bar{v}_v(t) = \text{col}(\dot{p}_v(t), 0)$, where the col operator indicates vertical stacking of column vectors to a combined column vector.

3.2 Fishing Gear

A real-world vessel is connected to trawl gear, which consists of flexible wires, trawl doors, net(s), winches, and other equipment. We significantly simplify the description to get an approximate model of the fishing gear's location in the ocean space.

Let $p_n(t), v_n(t) \in \mathbb{R}^3$ be the position and velocity of the net opening centroid given in {NED}. We connect $p_n(t)$ and $p_v(t)$ with a spring-damper system with nominal length $l_n(t) \in [l_{n,\min}, l_{n,\max}] =: \mathbb{X}_l$. The dynamics of the net opening is

$$\dot{p}_n(t) = v_n(t), \tag{2a}$$

$$\dot{v}_n(t) = \frac{F_n(t)}{m_n}, \tag{2b}$$

$$\dot{l}_n(t) = u_n(t), \tag{2c}$$

$$p_n(t_0) = p_{n,0},\ v_n(t_0) = v_{n,0},\ l_n(t_0) = l_{n,0}, \tag{2d}$$

$$l_n(t) \in \mathbb{X}_l, \tag{2e}$$

where $F_n(t) \in \mathbb{R}^3$ is the resultant force on a point mass with mass m_n and location $p_n(t)$, and $u_n(t) \in [u_{n,\min}, u_{n,\max}] =: \mathbb{U}_n$ is a constrained control input. Let $v_c(t) \in \mathbb{R}^3$ be the known water current. The forces acting on the point mass are: gravity f_g, buoyancy f_b, hydrodynamic drag $f_h(t, v_n, v_c)$, spring force $f_k(t, l_n, p_n, p_v)$, damping force $f_d(t, v_n, v_v)$, and cross-track stabilizer $f_q(t, p_n, p_v, \chi_v)$. Define $\hat{p}_{nv}(t) = (\bar{p}_v - p_n)/\|\bar{p}_v - p_n\|_2$, which is a unit vector pointing from p_n toward $\bar{p}_v$. The forces are

$$f_g = m_n g \begin{bmatrix} 0 & 0 & 1 \end{bmatrix}^\mathsf{T}, \tag{3a}$$

$$f_b = -m_n g \frac{\rho_w}{\rho_n} \begin{bmatrix} 0 & 0 & 1 \end{bmatrix}^\mathsf{T}, \tag{3b}$$

$$f_h(t, v_n, v_c) = \frac{1}{2} \rho_w A C_d \|v_c - v_n\|_2 (v_c - v_n), \tag{3c}$$

$$f_k(t, l_n, p_n, p_v) = k_n(\|\bar{p}_v - p_n\|_2 - l_n)\hat{p}_{nv}, \tag{3d}$$

$$f_d(t, v_n, v_v) = d_n\left((\bar{v}_v - v_n) \cdot \hat{p}_{nv}\right)\hat{p}_{nv}, \tag{3e}$$

where the dot $\cdot$ indicates the inner product, and parameters are defined in Table 1. Except the two first constants in the table, the remaining constants are considered variables to be determined. In particular, parameter identification using high-fidelity models or field trials, combined with sound judgment, should be performed to obtain values that give desired behavior of the simplified model.

Cross-Track Stabilizer There is a pendulum-like response between the net point and the vessel. The cross-track angle $\varphi(t)$ between the vessel's velocity vector and $\hat{p}_{nv}$ projected onto the xy-plane may become undesirably

[1] Defined in *Cross-Track Stabilizer*.

Table 1 Physical Parameters of Fishing Gear

Description	Symbol
Standard gravity	g
Water density	ρ_w
Gear point mass density	ρ_n
Area drag coefficient	AC_d
Spring coefficient	k_n
Damper coefficient	d_n
Gear total mass	m_n
Stabilizing force constant	q_n [1]

large during aggressive maneuvers. A too aggressive maneuver can cause the trawl net opening to collapse, which is a catastrophic event. For this reason it may be of interest to put a constraint on this angle. The projection of $\hat{p}_{nv}$ onto the xy-plane is

$$p_{nv,xy}(t) = \hat{p}_{nv} - (\hat{p}_{nv} \cdot e_z)e_z, \tag{4}$$

where $e_z = \text{col}(0, 0, 1)$ is a basis vector. Let $\hat{p}_{nv,xy}$ be the normalized vector of $p_{nv,xy}$. Using the inner product between $\hat{p}_{nv,xy}(t)$ and the normalized $\hat{\bar{p}}_v(t)$, the cosine of φ becomes

$$z_v(t, p_n, p_v, \chi_v) = \cos\varphi := \hat{p}_{nv,xy} \cdot \hat{\bar{p}}_v. \tag{5}$$

Suppose $\varphi \in [-\varphi_{\max}, \varphi_{\max}]$ must hold, so we arrive at the constraint requirement

$$z_v(t, p_n, p_v, \chi_v) \in [\cos\varphi_{\max}, 1]. \tag{6}$$

A real-life trawl net is connected to trawl doors, which open the net. During turning, the outer door attains higher speed than the inner door and therefore contributes to the net's tendency to shift outward. This phenomenon does, to some extent, stabilize the cross-track angle. Our simplified model mimics the stabilizing tendency with a planar force proportional to $\sin(\varphi)$ and perpendicular to $p_{nv,xy}$ defined as

$$f_q(t, p_n, p_v, \chi_v) = q_n \underbrace{\left(\hat{\bar{p}}_v \times \hat{p}_{nv,xy}\right)^{\mathsf{T}} e_z}_{\sin(\varphi)} \begin{bmatrix} 0 & -1 & 0 \\ 1 & 0 & 0 \\ 0 & 0 & 1 \end{bmatrix} \hat{p}_{nv,xy}, \tag{7}$$

where $q_n > 0$ is the stabilizing force constant and $\times$ is the cross product.

3.3 Fish Schools

The information one receives from a sonar about fish schools are usually the ones given in Table 2, see e.g. [16]. We can use this data when describing fish schools in a simplified manner. The shape of a school depends on several factors, including species, number of individuals, and velocity [17]. We assume that a fish school's shape can be approximated when its species, biomass, area, and velocity are known. Let us model a fish school as a collection of points that moves with uniform velocity. Each point has its own mass that represents a sub-volume of the school.

Table 2 Key Information About a Fish School

Description	Symbol
Position	$p_s \in \mathbb{R}^3$
Planar velocity	$v_{s,xy} \in \mathbb{R}^2$
Projected area	$A_{s,xy} > 0$
Mass	$M_s > 0$

Suppose you are given the information in Table 2 about a fish school, which has known species. Let $V_s \subset \mathbb{R}^3$ be the inferred bounding volume of the fish school, which has geometric center p_s, decomposed in the {NED} reference frame. We want to find a set of points that tessellate the fish volume and therefore proceed by defining an axial coordinate system for a face-centered cubic lattice as

$$p_{\text{fcc}} : \mathbb{R}^3 \to \mathbb{R}^3, \tag{8a}$$

$$w \mapsto p_s + 2\frac{\sqrt{3}}{3} r_s \begin{bmatrix} 1 & -1 & -1 \\ 1 & -1 & 1 \\ 1 & 1 & -1 \end{bmatrix} w, \tag{8b}$$

where $r_s > 0$ is a scalar constant[2]. Fig. 3a shows the spanning directions of the lattice. The set of points inside V_s, excluding points whose distance to the boundary are less than r_s, can be defined using the above lattice as

$$\begin{aligned} \mathcal{Q} := &\{z \in \mathbb{Z}^3 : p_{\text{fcc}}(z) \in V_s\} \setminus \\ &\{z \in \mathbb{Z}^3 : \inf\{x \in \partial V_s : \|x - p_{\text{fcc}}(z)\|_2\} < r_s\}, \end{aligned} \tag{9}$$

which is a set of 3-tuple integer coordinates, where ∂V_s is the boundary of V_s, see Fig. 3b. For each $\xi \in \mathcal{Q}$, $p_{\text{fcc}}(\xi)$ is the center of a sphere with radius r_s in a cubic close packing of spheres [18]. Let $n_s = |\mathcal{Q}|$ denote the number of points representing the fish school. If we assume uniform bounding volume density, each point approximately represents a spheric fish volume $V_\circ = 4\pi r_s^3/3$ with mass $m_s = M_s/n_s$.

Define ζ as the number of fish schools. For each $i \in \mathbb{I}_\zeta$, $\xi \in \mathcal{Q}_i$, declare the mass dynamics' right-hand

[2] This result can be achieved using a regular 3-simplex (tetrahedron) with an arbitrary orientation in Euclidean 3-space as a starting point. Let the geometric center of the tetrahedron be the origin with 2-norm distance $2r_s$ to any of the four vertexes. Pick three vertexes and find their Cartesian coordinates. These vectors constitute a spanning set for the axial coordinate system.

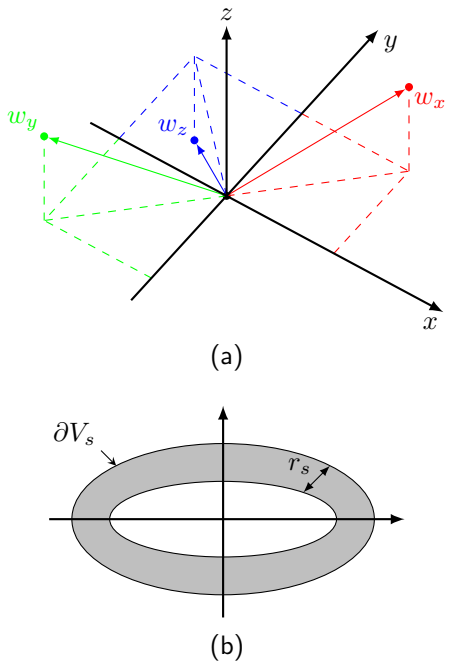

Fig. 3 (a) Face-centered cubic lattice spanning directions. The symbols w_x, w_y, w_z indicate coordinate vectors for $[1,0,0]^\mathsf{T}, [0,1,0]^\mathsf{T}, [0,0,1]^\mathsf{T}$, respectively;
(b) Plane intersection of a possible volume V_s with boundary ∂V_s. The shaded band indicates the region inside the volume at which coordinates will not be part of $\mathcal{Q}$.

side and the corresponding initial mass of its point with coordinate ξ as

$$f_{i,\xi} : \mathbb{R}_{\geq 0} \times \mathbb{R}^3 \times \mathbb{R} \to \mathbb{R}, \tag{10a}$$

$$m_{i,\xi}(t_0) = m_{i,s}. \tag{10b}$$

The time-varying position of this point is $\forall t \geq t_0$

$$p_{i,\xi}(t) = p_{i,\text{fcc}}(\xi) + v_{i,s}(t - t_0), \tag{11}$$

where $v_{i,s} = \text{col}(v_{i,s,xy}, 0)$. Each point mass will have a dynamic response on its mass that depends on the position of the net opening $p_n(t)$ and its orientation. Although we have restricted the description of the fish school movement to uniform velocity, this assumption can be relaxed. For instance, if the centroid mass point moved with a description similar to that of the vessel (1), all points would need to satisfy the movement as a rigid body. This is because their relative position cannot change if the points are to retain the property as a cubic close packing of spheres.

Let us first elaborate on how to model the trawl catch dynamics, before we resume to the definition of the mass differential equation in Section 3.4.2.

3.4 Trawl Catch Dynamics

The interaction between the trawl net opening and the fish schools is important for quantifying the reward of the harvest. This mechanism involves the boundary of the net opening and the movement of each individual in the fish school. It therefore requires detailed descriptions of both each individual's behavior and the net to determine catch or no catch with high accuracy. Inspired by [10], we propose instead a reaction-like response of each point mass in the fish school if it is sufficiently close to the net opening centroid. The net behaves as a 'consumer' of fish mass. The rate of consumption increases as the distance between the net and a fish point mass reduces. Next, we define some mathematical expressions based on bell-shaped exponential functions, which is used to describe the desired behavior.

Let $w \in \mathbb{R}$ and $\sigma, r \in \mathbb{R}_{>0}$. Consider the symmetric exponential function

$$f_{\text{exp}}(w) = \exp\left(-\frac{w^2}{a(\sigma, r)}\right), \tag{12}$$

where $a(\sigma, r)$ is a constant to be determined. Suppose that $f_{\text{exp}}(\sigma + r) = c$, where $c \in]0, 1[$ is a desired gain. Solving (12) with respect to a gives

$$a(\sigma, r) = -\frac{(\sigma + r)^2}{\ln c}. \tag{13}$$

The resulting function f_{exp} is a bell-shaped exponential function with gain c at $w = \sigma + r$. We take the tensor product of three exponential functions to get a gain function with ellipsoidal level surfaces. Let $\sigma_1, \sigma_2, \sigma_3 \in \mathbb{R}_{>0}$, r, and c be given constants, written together as $\vartheta = \text{col}(\sigma_1, \sigma_2, \sigma_3, c)$. For $w \in \mathbb{R}^3$ we get

$$K(\vartheta, r) = \text{diag}\left(\frac{1}{a(\sigma_1, r)}, \frac{1}{a(\sigma_2, r)}, \frac{1}{a(\sigma_3, r)}\right), \tag{14a}$$

$$f_{\text{exp},3}(w; \vartheta, r) = \exp\left(-w^\mathsf{T} K(\vartheta, r) w\right). \tag{14b}$$

Fig. 4 shows a snapshot of a simulation where the ellipsoidal level surface represents the net opening.

3.4.1 Distance Gain

We want to place the newly defined gain function at the net opening, so that it constitutes the net's actuator on the fish masses. The net opening is assumed to be perpendicular to the planar orientation of the link that connects to the vessel. Let $\{\text{T}\}$ denote a Cartesian coordinate system with origin $p_n(t)$ and x-axis pointing along the normalized $\hat{p}_{nv,xy}(t)$ and z-axis along

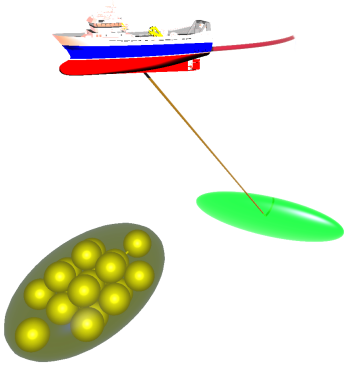

Fig. 4 A snapshot of a 3D simulation with a vessel, net opening and an ellipsoidal fish school, which is tessellated with a cubic close packing of spheres. Spheres with volume outside the ellipsoid are excluded.

{NED}'s z-axis. Let $\theta(t)$ be the angle rotation from the x_{NED}-axis to the x_{T}-axis. We can write

$$\cos\theta = e_x \cdot \hat{p}_{nv,xy}, \tag{15a}$$

$$\sin\theta = (e_x \times \hat{p}_{nv,xy})^{\mathsf{T}} e_z, \tag{15b}$$

$$R(\theta) = \begin{bmatrix} \cos\theta & -\sin\theta & 0 \\ \sin\theta & \cos\theta & 0 \\ 0 & 0 & 1 \end{bmatrix}, \tag{15c}$$

where $R(\theta)$ is the rotation matrix that transforms vectors given in {T} to {NED} and e_x, e_y, and e_z are basis vectors. Consider the coordinate $w_{\text{NED}} \in \mathbb{R}^3$ decomposed in the {NED} frame. The coordinate transformation to {T} is

$$w_{\text{T}} = R^{\mathsf{T}}(\theta)(w_{\text{NED}} - p_n), \tag{16}$$

so, if we substitute this expression into (14b), we get a gain function for coordinates w given in {NED}:

$$f_\gamma(t, w, p_n, \theta; \vartheta, r) = \exp\left(-(w - p_n)^{\mathsf{T}} R(\theta) K(\vartheta, r) R^{\mathsf{T}}(\theta)(w - p_n)\right). \tag{17}$$

The parameter vector ϑ can be set to produce an ellipsoidal level surface that approximately covers the trawl net's opening with a specific c gain and thereby behaves as a reaction-like actuator on point masses with radius r. The closer a point mass is to the net opening centroid, the larger the reaction gain.

3.4.2 Fish School Mass Dynamics

We are now ready to define how the fish schools' masses are affected by the trawl net. Consider a volume with radius r_s, initial mass $m_{s,0}$, center position $p(t) \in \mathbb{R}^3$, and velocity $v_s(t) \in \mathbb{R}^3$. The trawl net model influences this mass in the following manner

$$\dot{m}_s(t) = -\gamma f_\gamma(t, p, p_n, \theta; \vartheta, r_s) m_s, \tag{18}$$

where $\gamma > 0$. This models a maximal amount of caught fish when the net centroid is swept through the volume center.

Define for each fish school $i \in \mathbb{I}_\zeta$ the mass state vector $m_i(t) := \text{col}_{\xi \in \mathcal{Q}_i}(m_{i,\xi}(t)) \in \mathbb{R}^{|\mathcal{Q}_i|}$ with lexicographical ordering according to ξ and stacked time-varying position vector $p_i(t) := \text{col}_{\xi \in \mathcal{Q}_i}(p_{i,\xi}(t))$. We apply (18) on all mass points of all fish schools, so that $\forall i \in \mathbb{I}_\zeta$

$$A_i(t, p_i, p_n, \theta; \vartheta, \varsigma_i) = \text{diag}_{\xi \in \mathcal{Q}_i}(-\gamma f_\gamma) \tag{19}$$

is a $|\mathcal{Q}_i| \times |\mathcal{Q}_i|$ negative definite matrix, where we have defined $\varsigma_i = \text{col}_{\xi \in \mathcal{Q}_i}(r_{i,\xi})$, and

$$\dot{m}_i(t) = A_i(t, p_i, p_n, \theta; \vartheta, \varsigma_i) m_i, \tag{20a}$$

$$m_i(t_0) = \text{diag}_{\xi \in \mathcal{Q}_i}(m_{i,\xi}(t_0)), \tag{20b}$$

is the mass dynamics for fish school i. This model does not take into account mass redistribution within a school during catch. It is, however, straightforward to extend the model with for instance a semi-discretized diffusion equation. A reshaping and shrinking bounding volume is a more complicated matter that is not easily incorporated into this model.

Remark 1 *By using a close packing of spheres with uniform radius as outlined in* (8)*, the radii of point masses within a single school are identical. Hence,* ς_i *is uniform with the common radius* $r_{i,s}$*.*

3.5 Fish Harvest Indication

In our description, the reduction of mass in a school equals a corresponding increase of harvested mass. Denote $\varpi : \mathbb{R}_{\geq t_0} \to \mathbb{R}_{\geq 0}$ as harvested mass. The harvested mass function is thus

$$\varpi(t) = \sum_{i \in \mathbb{I}_\zeta, \xi \in \mathbb{Q}_i} (m_{i,\xi}(t_0) - m_{i,\xi}(t)). \tag{21a}$$

3.6 Dynamic Optimization Problem

The *Path Planner* makes use of the models described in the previous sections. Define the control input vector $u(t) := \text{col}(u_v, u_n) \in \mathbb{U} := \mathbb{U}_v \times \mathbb{U}_n$. The objective is formulated as an optimal control problem (OCP) of *Bolza*-type, such that $\forall i \in \mathbb{I}_\zeta$, $\forall t \in [t_0, t_f]$

$$\min_{u \in \mathbb{U}} \quad \int_{t_0}^{t_f} u^{\mathsf{T}}(t) \Lambda u(t)\, \mathrm{d}t - \eta \varpi(t_f) \tag{22a}$$

$$\text{s. t.} \quad (1), (2), (6), (20), \tag{22b}$$

where Λ and η are positive definite tuning variables. This control problem tries to maximize harvest ϖ at

the end of the time horizon, while at the same time being conservative with the control inputs, namely, vessel turning and winch activity. Denote the solution to (22) as $u^\star(t) : [t_0, t_f] \to \mathbb{U}$, which plugged into the initial value problems (1) and (2), gives desired trajectories $p_v^\star(t)$ and $p_n^\star(t)$ for the vessel and net opening, respectively. These trajectories are maneuvering tasks for the vessel and winch path-tracking control systems.

3.7 Solution Strategies for the Path Planning Problem

3.7.1 Regularization

The reaction gain (17) is exponentially decaying with increasing distance between the net and a school. A consequence of this property is that the local iterative algorithm may not understand (i.e. there is no gradient) that moving toward a distant school is beneficial. To overcome this issue, we extend the formulation with a regularizing term

$$f_{\text{reg}}(t, w, p_n, \theta; \vartheta_2, r) = \gamma_2(1 - f_\gamma(t, w, p_n, \theta; \vartheta_2, r)), \tag{23}$$

where ϑ_2 and γ_2 are tuning variables. The rationale behind this function is that it helps the net seeking toward distant schools. Note that this term is also based on an exponential function, but by choosing ϑ_2 appropriately large, it will not vanish in the desired region of operation. We add the school-seeking term to the centroid point mass dynamics of each school. For each $i \in \mathbb{I}_\zeta$, the centroid mass dynamics becomes

$$\dot{m}_{i,0}(t) = -\gamma f_\gamma m_{i,0} + f_{\text{reg}}(t, p_{i,0}, p_n, \theta; \vartheta_2, r_{i,0}). \tag{24}$$

A downside of f_{reg} is that it is an artificial source, so the mass will slowly increase when the net is far away.

3.7.2 Conditioning

The exponential expression (14b) can give numerically ill-conditioned derivatives for large-valued optimization variables. To improve conditioning, all position variables have been scaled by a factor λ, so $p_s = \lambda p$ is the scaled position.

3.7.3 Receding Horizon

The proposed OCP (22) grows with time horizon length and will eventually become computationally too expensive for practical applicability. Moreover, changing ambient conditions and modeling uncertainties motivate the need for periodic re-planning. We therefore solve the problem in a receding horizon fashion. For iteration j, we optimize over a finite horizon $\mathbb{T}_j = [t_{j,0}, t_{j,f}]$ and realize a sub-interval $\mathbb{T}_{j,c} = [t_{j,0}, t_{j,c}]$, denoted the control horizon, where $t_{j,c} < t_{j,f}$. The subsequent interval starts with $t_{j+1,0} = t_{j,c}$.

3.7.4 Implementation

We employ a direct transcription approach that discretize both the state and control variables into a finite-dimensional nonlinear programming (NLP) problem. We use simultaneous collocation of finite elements to get Lagrange interpolation polynomial descriptions of the state variables. The control input are piecewise linear. For details on collocation, consult [19, 20]. The resulting discrete problem is large, but also sparse with structure. We therefore implement the problem in the symbolic framework CasADi 2.4.1 [21] and use the primal-dual interior-point NLP solver IPOPT 3.12.0 [22], with OpenBLAS 0.2.13 [23] and the linear algebra sparse solver MA57 3.7.0 [24] from HSL.

3.7.5 Constrained Control Input

The control signals $u_v(t)$ and $u_n(t)$ are speed signals for yaw and winch. A bounded piecewise linear signal that are connected across elements will ensure that the acceleration is bounded. We achieve this by constraining both u and its time derivative within each collocated element as follows. Consider element e with a control input $u_e : [0, h] \to [u_{\min}, u_{\max}]$. The following equations

$$u_e(t) = a + bt, \tag{25a}$$
$$u_e(h) = u_{e+1}(0), \tag{25b}$$
$$a \in [u_{\min}, u_{\max}], \qquad b \in [u_{\min}^t, u_{\max}^t], \tag{25c}$$

ensure a bounded signal with bounded derivatives, as long as the subsequent element also obeys the bounds.

4 Case Study

We explore the proposed path planner in an example consisting of two ($\zeta = 2$) fish schools that move with constant velocity. Configuration parameters and variables for the simulation are selected for demonstrating the method more than representing a specific trawl system, and the numerical results are presented.

4.1 Setup

4.1.1 Vessel

The forward speed is $U = 2\,\text{m}\,\text{s}^{-1}$, and the initial conditions are $p_{v,0} = \text{col}(0, 0)$ and $\chi_{v,0} = 0$. The yaw

Table 3 Parameters Relevant to the Fishing Gear

Symbol	Value	Unit
g	9.81	$\mathrm{m\,s^{-2}}$
ρ_w	1000	$\mathrm{kg\,m^{-3}}$
ρ_n	4000	$\mathrm{kg\,m^{-3}}$
AC_d	10	$\mathrm{m^2}$
m_n	2000	kg
k_n	10^7	$\mathrm{kg\,s^{-2}}$
d_n	$2\sqrt{k_n m_n}$	$\mathrm{kg\,m^{-1}\,s^{-1}}$
q_n	5000	N

rate input is set to be piecewise linear with bounds $u_v \in [-0.03, 0.03]$ and $\frac{du_v}{dt} \in [-10^{-3}, 10^{-3}]$.

4.1.2 Gear

The net centroid is set to have initial conditions $p_{n,0} = \mathrm{col}(-165.83, 0, 250)$, $v_{n,0} = \mathrm{col}(2, 0, 0)$, and $l_{n,0} = 300$. The ocean current is constant $v_c(t) = \mathrm{col}(0.5, 0, 0)$. Other relevant parameters are found in Table 3. Determining parameters without a high-fidelity model is difficult because they represent the aggregation of complex behavior into a simple model. The following characteristics where considered when running simulations that helped selecting the indicated parameters in Table 3:

- The lift from the doors and the net drag make net opening lag behind the vessel and pulled toward the surface. Tuned with ρ_n and AC_d.
- The doors dampen lateral motion during turning. Tuned with q_n.
- The warps have a catenary curve between the vessel and doors, which indicates a spring-damper-like response between them. Tuned with k_n and d_n, where k_n was chosen to be much softer than a e.g. steel wire.
- The water drag dampens oscillatory motion. Tuned with all damping parameters and m_n. We chose d_n to get a critically damped response.

By exploiting the physical characteristics of components in the low-fidelity model, we can hand-tune the parameters to get a desired response in the simulation model. For instance, we ran straight-line and turning maneuvers to scrutinize both the vertical and horizontal response of the net position. The winch speed input is piecewise linear with $u_n \in [-0.4, 0.4]$ and $\frac{du_n}{dt} \in [-0.1, 0.1]$. The link length is constrained to $\mathbb{X}_l := [150, 500]$ and $\varphi_{\max} = 45°$.

4.1.3 Schools

Each school is approximated by a single ($n_s = 1$) point mass situated in the origin of an ellipsoid, which is the assumed bounding volume of the fish school. Relevant parameters for the schools are given in Table 4. The schools are set up to capture a scenario where the fishes congregate in limited sizes. This is a common scenario when fishing for blue whiting early in the year/season [25, 26].

Table 4 Fish School Parameters

Symbol	School 1	School 2
i	1	2
$p_{i,0}(t_0)$	$\mathrm{col}(100, 50, 170)$	$\mathrm{col}(500, -150, 240)$
$v_{i,s}$	$\mathrm{col}(0, -1, 0)$	$\mathrm{col}(-0.5, 0.5, 0)$
$r_{i,s}$	25 m	25 m
$m_{i,s}$	3000 kg	3000 kg

4.1.4 Catch Dynamics

The catch parameters are $\vartheta = \mathrm{col}(10, 75, 40, 0.2)$ and $\gamma = 0.01$. The school-seeking regularization term has parameters $\vartheta_2 = \mathrm{col}(10^3, 10^3, 10^3, 0.2)$ and $\gamma_2 = 0.3$.

4.1.5 Optimization

Objective function parameters are $\Lambda = \mathrm{diag}(10^{-2}, 5 \times 10^{-3})$ and $\eta = 1$. The optimization problem is set up with a horizon of $(t_{j,f} - t_{j,0}) = 200\,\mathrm{s}$ and control horizon of $(t_{j,c} - t_{j,0}) = 60\,\mathrm{s}$. The element time width is 10 s, which gives 20 collocation elements. Within each element the control inputs are linear and the states are discretized with Radau collocation of degree 2. Conditioning variable $\lambda = 10^{-2}$. There are in total 812 optimization variables. The simulation runs for a total of 17 control horizons, which gives results in 1020 s of simulated time.

4.2 Numerical Results

The receding horizon optimization problem was solved on a Intel Core i5-4250U with 8 GB of memory. Computation times for each optimization problem can be found in Fig. 5. All problems solved well within the control horizon of 60 s.

The planar positions of the vessel, net, and fish schools are shown using a North-East plot in Fig. 6. We see that the planned path first approached School 1, then School 2. The corresponding mass of each school is given in Fig. 7. We see that the mass of each school reduced rapidly in a limited time interval, indicating that the fishing net consumed mass from the matching school.

In Fig. 8 the optimal yaw rate and winch speed are displayed from top to bottom, respectively. We see that

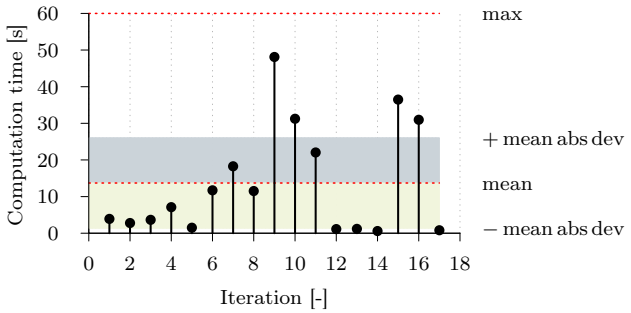

Fig. 5 The computation time for each optimization problem. All problems solved within the control horizon, which is 60 s.

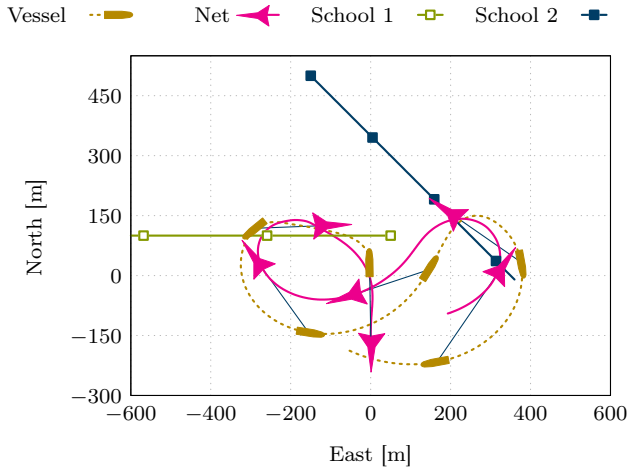

Fig. 6 The planar positions of the vessel, net, and fish schools. The vessel and net's locations are indicated with icons every 3 min.

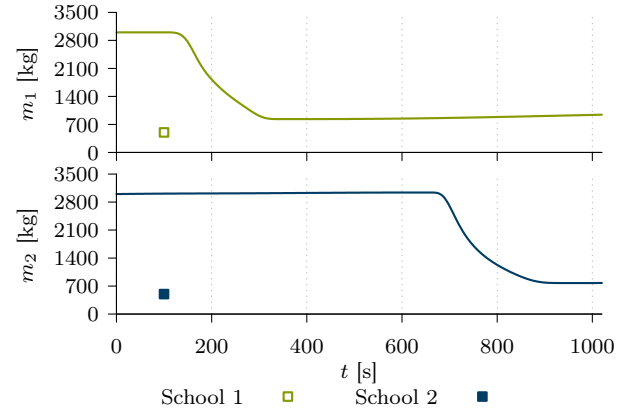

Fig. 7 The mass of each school. The top plot is School 1, while the bottom plot is School 2. The reduction of mass is due to trawl sweaps.

the yaw rate was occasionally on the constraint boundary, whereas the winch speed more often operated at the limits of allowed speed. The resulting time series of the link length between the vessel and the net is given in Fig. 9. We see that the wire length never was close

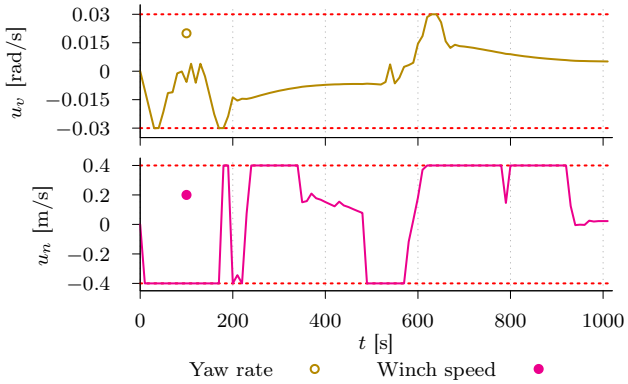

Fig. 8 The control inputs resulting from the receding optimization. The dashed red lines indicate bounds in the control signals. The upper figure shows the yaw rate, while the bottom figure shows the winch speed.

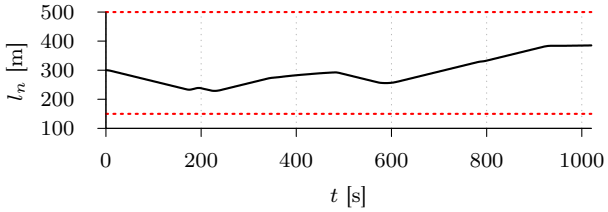

Fig. 9 The length of the link between the vessel and the net. The dashed red lines are bounds on wire length.

to the prescribed constraints, which are indicated by dashed lines. The wire length is a contributing factor for controlling the depth of the net. In order to ensure harvest, the depth of the net must be sufficiently close to a school. In Fig. 10 we see the depth of each school and the time-varying net depth. By simultaneously conferring Fig. 7, we see that the net's depth coincided (approximately) with a school's depth when it was harvested. One reason why the commanded winch speed at times exhibits 'bang-bang'-like control is that maximization of harvest dominates penalization of control input in the objective function (with the chosen optimization parameters). A curious observation with the current formulation is that the planner pays out or in winch length in order to minimize the net-to-school distance. This phenomenon can particularly be observed by inspecting Figs. 9 and 10 from about 700 s, as the vessel is actually moving away from School 2.

The path planner avoided too aggressive maneuvers, since the angle between the vessel velocity and the planar link projection never exceeded 45°, see Fig. 11. Observe that the maximal angle was a reality for a considerable fraction of the simulated time.

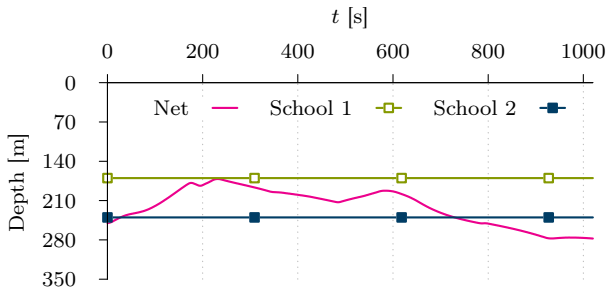

Fig. 10 The figure shows the time-varying depth of the net centroid together with school centroids. The net depth depends on wire length, but also the maneuvering of the vessel.

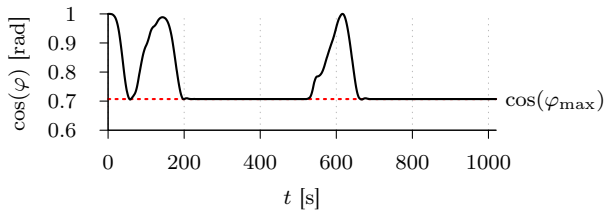

Fig. 11 The angle between the vessel velocity and the planar link projection. $\varphi \leq \varphi_{\max} = 45°$ is achieved using the path planner.

5 Discussion

The presented algorithm successfully finds feasible trajectories that lead to harvest of the fish schools in real time. However, there are some issues that should be pointed out. We present trawl catch dynamics that only depends on the distance between the net and a fish point mass. This would indicate that minimization of the distance between the net and the fish mass point(s) results in the best harvest rate. This is not correct. A better model should also include the relative sweep velocity between the net and the fish points. In particular, the harvest rate should be maximal when the net is close to a fish mass point and sweeps across the point with an 'optimal' speed, neither too fast nor too slow. Such a description would make the problem more challenging to solve.

Another concern with the formulation is its scalability. We have already limited the problem size by applying a bounded horizon size, which can result in greedy solutions. The presented simulation exhibits real-time capabilities on under-powered hardware, but this may quickly change for increasing number of school points. This may not be a big problem for the intended application, since in a harvest operation there is rarely focus on more than two or three schools at the same time. Nevertheless, if one were to use multiple points for each school (as described in Section 3.3), which may be relevant for huge fish schools, computation challenges will arise. This challenge may possibly be somewhat alleviated by choosing a different solution approach, for instance by separating the system into a formulation with both shooting and collocation descriptions [27].

The optimization problem may not solve within the nominal time limit, which is the control horizon. One may create mechanisms for aborting and trying a reformulated optimization problem with a secondary time limit (like the final optimization time point of the previous iteration). There is no guarantee that an optimal solution will be found. As long as the purpose of the system is to lessen the burden for the captain, human intervention is a viable failure mitigation mechanism. Entering a predefined 'safe' solution until a optimization succeeds may also be an alternative.

A benefit of the proposed formulation is its flexibility of adding more constraints and other descriptions. It is straightforward to add useful properties, such as limiting the harvest rate, since harvesting fish too fast may rupture the net, and avoidance constraints, either collision with other vessels or capture of undesired fish schools. Knowledge of other vessels and fish schools are easily obtained from radar or sonar measurements. Safety in a shared robots-human space [8] is a highly relevant challenge for this application.

One possible validation strategy for the motion planning method is to make use of high-fidelity models describing the vessel, trawl gear, fish schools, and fish-net interaction as a simulator for a real-world scenario. The role of full-scale data may be to parameterize the high-fidelity models. The benefit of a simulator is its repeatability: Both manual operation with an experienced captain, as well as autonomous motion planning can be executed on the same capture scenarios for comparison.

6 Conclusion

We have proposed a motion planning system for autonomous trawling. This work can contribute in making the tactical harvest phase more efficient. Moreover, it is a step toward reducing human intervention in trawling through seamless utilization of information about the surroundings in the motion planning. Our formulation demonstrates motion planning of a robot (vessel) with an actuator (fishing net) that interacts with the surroundings (fish schools). We have advocated the flexibility of the formulation, and stated that extensions can be uncomplicated. The system can also be adapted to problems with similar composition. Challenges still remain, in particular, the formulation needs further work on a solution approach for mitigating com-

putational scalability issues, as well as definition of robustness mechanisms to enable practical usefulness.

A Path Planner Variable Descriptions

Table 5 gives a short description of the variables and parameters used in the path planner formulation, while Table 6 does the same for the optimal control problem formulation.

Table 5 Path Planner Variable Descriptions

Fishing Vessel	
Description	Symbol
Position	$\bar{p}_v(t) \in \mathbb{R}^3$
Velocity	$\bar{v}_v(t) \in \mathbb{R}^3$
Course	$\chi_v(t) \in \mathbb{R}$
Planar speed	$U > 0$
Rate of turn	$u_v(t) \in \mathbb{U}_v$
Fishing Gear	
Description	Symbol
Net opening position	$p_n(t) \in \mathbb{R}^3$
Net opening velocity	$v_n(t) \in \mathbb{R}^3$
Relaxed length $\bar{p}_v$ to p_n	$l_n(t) \in \mathbb{X}_l$
Net point mass	$m_n > 0$
Resultant force on p_n	$F_n(t) \in \mathbb{R}^3$
Rate of change of l_n	$u_n(t) \in \mathbb{U}_n$
Water current	$v_c(t) \in \mathbb{R}^3$
Angle between v_v and $p_{nv,xy}$	$\varphi(t) \in [-\varphi_{\max}, \varphi_{\max}]$
Net-to-vessel vector, projected onto the xy-plane, normalized	$\hat{p}_{nv,xy} \in \mathbb{R}^3$
Cosine of φ	$z_v \in [\cos(\varphi_{\max}), 1]$
Fish Schools	
Description	Symbol
Bounding volume of school	$V_s \subset \mathbb{R}^3$
Boundary of V_s	∂V_s
Centroid of school	$p_s \in \mathbb{R}^3$
Mass of school	M_s
Set of points inside bounding volume	$\mathcal{Q}$
Number of points in $\mathcal{Q}$	n_s
An element in $\mathcal{Q}$	$\xi \in \mathcal{Q}$
Radius of a sphere	r_s
Mass of a sphere	m_s
Center of sphere ξ	$p_{\text{fcc}}(\xi)$
Number of fish schools	ζ
Mass of sphere element ξ in school i	$m_{i,\xi}(t)$
Trawl Catch Dynamics	
Angle of {T} relative to {NED}	θ
Parameter vector for ellipsoidal level surface	ϑ
Ellipsoidal level surface	$f_\gamma(t, w, p_n, \theta; \vartheta, r)$
Mass-net gain parameter	$\gamma > 0$
School i's mass-net reaction system matrix	$A_i(t, p_i, p_n, \theta; \vartheta, \varsigma_i)$
Fish Harvest Indication	
Total harvested mass	$\varpi(t) \in \mathbb{R}_{\geq 0}$

References

1. K.J. Reite, Modeling and Control of Trawl Systems. Ph.D. thesis, Norwegian Univ. Sci. & Technol., Trondheim, Norway (2006). URL http://hdl.handle.net/11250/237617
2. C.W. Lee, Fisheries Research **24**(4), 311 (1995). DOI 10.1016/0165-7836(95)00388-2
3. C.W. Lee, J.H. Lee, I.J. Kim, Fisheries Sci. **66**(5), 858 (2000). DOI 10.1046/j.1444-2906.2000.00139.x
4. C.W. Lee, C.I. Zhang, H.O. Shin, Fisheries Research **53**(1), 83 (2001). DOI 10.1016/S0165-7836(00)00264-2
5. Y.l. Chen, H. Zhou, Y.g. Zhao, J.y. Hou, J. Central South Univ. **21**(1), 167 (2014). DOI 10.1007/s11771-014-1928-1
6. C.W. Lee, Fish. sci. **68**(sup2), 1835 (2002). DOI 10.2331/fishsci.68.sup2_1835
7. S.M. LaValle, *Planning Algorithms* (Cambridge Univ. Press, New York, NY, 2006)
8. A. Khan, B. Rinner, A. Cavallaro, IEEE Trans. Cybern. **PP**(99), 1 (2016). DOI 10.1109/TCYB.2016.2628161
9. J. Haugen, L. Imsland, Unmanned Systems **3**(3), 221 (2015). DOI 10.1142/S2301385015500144
10. J. Haugen, L. Imsland, IEEE Trans. Control Syst. Technol. **24**(2), 475 (2015). DOI 10.1109/TCST.2015.2454432
11. J. Haugen, E. Grimaldo, S.H. Gjøsund, in *ASME 2017 36th International Conference on Ocean, Offshore and Arctic Engineering* (American Society of Mechanical Engineers, 2017), pp. V07BT06A025–V07BT06A025
12. D. Priour, in *Proc. 12th Int. Congr. Int. Maritime Association Mediterranean, IMAM 2005 – Maritime Transportation and Exploitation Ocean and Coastal Resources*, vol. 2 (2005), vol. 2, pp. 1285–1292. URL http://www.ifremer.fr/web-com/dpriour/web/papers/2005_lisbon_FEM.pdf
13. P. Lader, A. Fredheim, in *Proc. OOA IV Open Ocean Aquaculture IV Symposium* (2003). URL https://www.sintef.no/globalassets/upload/fiskeri_og_havbruk/havbruksteknologi/intellistruct/lader2001_modnetstruct_ooa.pdf
14. A. Fredheim, Current forces on net structures. Ph.D. thesis, Norwegian Univ. Sci. & Technol., Trondheim, Norway (2005). URL http://hdl.handle.net/11250/231260
15. T.I. Fossen, *Handbook of Marine Craft Hydrodynamics and Motion Control* (John Wiley & Sons Inc., Hoboken, NJ, 2011)
16. Simrad SX90 Fish Finding Sonar – Measured Data Shoal (2016). URL http://www.simrad.net/sx90/ref_english/xxx_telegram_own_mds.html
17. B. Partridge, T. Pitcher, J. Cullen, J. Wilson, Behav. Ecol. Sociobiol. **6**(4), 277 (1980). DOI 10.1007/BF00292770
18. E.W. Weisstein. Cubic close packing. From MathWorld – A Wolfram Web Resource (2015). URL http://mathworld.wolfram.com/CubicClosePacking.html
19. J.T. Betts, *Practical Methods for Optimal Control and Estimation Using Nonlinear Programming*, 2nd edn. (SIAM, Philadelphia, PA, 2010). DOI 10.1137/1.9780898718577
20. L.T. Biegler, *Nonlinear Programming: Concepts, Algorithms & Applications to Chemical Processes* (SIAM, Philadelphia, PA, 2010). DOI 10.1137/1.9780898719383
21. J. Andersson, J. Åkesson, M. Diehl, in *Recent Advances in Algorithmic Differentiation*, *Lecture Notes in Computa-*

Table 6 Dynamic Optimization Parameters

Dynamic Optimization Problem	
Gain matrix for control input	Λ
Tuning variable for harvest indication	$\eta > 0$
Optimized control input, turn rate and winch speed	$u^\star(t) \in \mathbb{U}$
Optimized vessel trajectory	$p_v^\star(t) \in \mathbb{R}^3$
Optimized net trajectory	$p_n^\star(t) \in \mathbb{R}^3$
Solution Strategies	
Regularizing level surface	f_{reg}
Regularizing gain	$\gamma_2 > 0$
Regularizing parameter vector for level surface	ϑ_2
Position scaling factor	$\lambda > 0$
Optimization horizon for iteration j	$\mathbb{T}_j$
Control horizon for iteration j	$\mathbb{T}_{j,c}$

tional Sci. and Eng., vol. 87, ed. by S. Forth, P. Hovland, E. Phipps, J. Utke, A. Walther (Springer-Verlag, Berlin Heidelberg, Germany, 2012), pp. 297–307. DOI 10.1007/978-3-642-30023-3_27

22. A. Wächter, L.T. Biegler, Math. Programming **106**, 25 (2006). DOI 10.1007/s10107-004-0559-y
23. Z. Xianyi, W. Qian, Z. Yunquan, in *Proc. IEEE 18th Int. Conf. Parallel and Distributed Syst. (ICPADS)* (Singapore, 2012), pp. 684–691. DOI 10.1109/ICPADS.2012.97
24. HSL. A collection of Fortran codes for large scale scientific computation. (2016). URL `http://www.hsl.rl.ac.uk`
25. K.J. Reite. Private Communication (2018)
26. P. Petitgas, D. Reid, P. Carrera, M. Iglesias, S. Georgakarakos, B. Liorzou, J. Masse, ICES J. Marine Sci. **58**, 1150 (2001). DOI 10.1006/jmsc.2001.1130
27. A. Albert, L. Imsland, J. Haugen, IFAC-PapersOnLine **49**(7), 290 (2016). DOI 10.1016/j.ifacol.2016.07.307. 11th IFAC Symp. Dynamics Control Process Syst. – Incl. Biosyst. DYCOPS-CAB – Trondheim, Norway, 6–8 June